Thesis for the degree
Master of Science

Submitted to the Scientific Council of the
Weizmann Institute of Science
Rehovot, Israel

עבודת גמר (תזה) לתואר
מוסמך למדעים

מוגשת למועצה המדעית של
מכון ויצמן למדע
רחובות, ישראל

By
Yotam Lifschytz

מאת
יותם ליפשיץ

מאפיינים משותפים של התפלגות הכשירות האבולוציונית במודלים שונים של מרחבי כשירות

Universal Features of Fitness Landscapes Across Fitness Landscape Models

Advisors:
Ariel Amir, Yitzhak Pilpel

מנחים:
אריאל אמיר, יצחק פלפל

August 2025

אב תשפ״ה

Abstract

Evolutionary trajectories of organisms are shaped by the distribution of fitness effects (DFE), which offers crucial insights into adaptive processes. Here, we analyze and compare DFEs that emerge from three of the most widely used fitness landscape models to explore commonalities with empirically observed DFE dynamics. We reproduce key empirical results observed by Couce et al. and others, such as the overall shape and dynamics of the DFE during adaptive walks, the exponential form of the distribution of beneficial fitness effects, global epistasis, and a phenomenon where the fitness effects of mutations decorrelate during the evolutionary process. We uncover striking qualitative convergence across these distinct models, suggesting a form of underlying universality across all fitness landscape models, and perhaps even across evolutionary processes, regardless of organism or environment details.

Contents

1 Introduction

Biological evolution is the process through which populations of organisms or proteins adapt to their environments over time. Central to this process is the variation introduced by mutations, which serve as the raw material for natural selection. To understand evolution at the molecular level, it is essential to distinguish between two key concepts: genotype and phenotype. The genotype represents an organism's genetic makeup—the specific sequence of nucleotides in its DNA. This sequence encodes the instructions for producing all proteins and RNA molecules within the organism. In contrast, the phenotype encompasses the observable traits of the organism, including its morphology, behavior, metabolic characteristics, and other measurable attributes. The relationship between genotype and phenotype is intricate and often many-to-one: different genotypes can produce similar phenotypes, and small genetic changes can lead to significant, minor, or negligible phenotypic effects [1]. Gene regulation plays a pivotal role in this mapping, determining when and how much of each gene product is expressed. Certain genotypes may result in phenotypes better suited to specific environments, while others may be maladaptive. For example, a genotype encoding a protein with high binding affinity for a substrate may confer an advantage in environments where the substrate is scarce but may be disadvantageous in environments where it is abundant. To formalize this concept, evolutionary biologists use the notion of fitness. Fitness, in its abstract form, is a function mapping genotypes to real numbers: $f : \mathcal{G} \to \mathbb{R}$, where $\mathcal{G}$ represents the space of all possible genotypes, and $f(g)$ quantifies the reproductive success—or adaptive value—of genotype g in a given environment. The manifold created by this function over genotypic space is often referred to as the fitness landscape [2]. Fitness is inherently abstract and not directly observable; it is inferred from the reproductive success of organisms with different genotypes. While fitness encompasses many factors, experimental studies often approximate it using growth rates or the relative abundance of a genotype within a population [2]. Although this is a practical proxy, it excludes important factors such as stress responses [2]. To explore the fitness landscape, organisms undergo mutations—changes to their genetic sequences. Point mutations involve the substitution of a single nucleotide for another, and insertions and deletions (collectively known as indels) add or remove small stretches of DNA. Larger-scale mutations include duplications, where entire genes or genomic regions are copied; inversions, where segments of DNA are flipped in orientation; and translocations, where parts of chromosomes are rearranged [3]. Mutations can arise spontaneously through errors in DNA replication or be induced by environmental factors such as radiation or chemical mutagens [3]. Mutations can have a wide range of effects on fitness, from neutral (no effect) to deleterious (harmful) to beneficial (advantageous). The structure of the fitness landscape depends on how mutations interact, including whether combinations of mutations produce synergistic or antagonistic effects — a phenomenon known as epistasis [4]. More specifically, epistasis refers to the interaction between mutations, where the effect of one mutation depends on the presence or absence of other mutations. When a mutation arises in a population, its fate — whether it disappears or becomes established — depends on the effect it has on fitness. This is usually referred to as the fixation probability; fixation being defined as the event in which a mutation spreads through the entire population, replacing the ancestral genotype.

Genotypic evolution can be understood as an optimization process in which organisms strive to maximize

their fitness across genotypic space. Evolution operates at the population level, with populations exploring genotypic space through mutation and selection, where the directed movement towards higher fitness is often referred to as an adaptive walk. However, evolution is a local optimization process, with mutations acting as the means to sample the local genotypic neighborhood; organisms have no access to the global properties of the fitness landscape. Each mutation has a fixation probability that depends on its fitness effect, and once a mutation fixes in the population, it alters the population's genotype, creating a new genotypic neighborhood. The distribution of fitness effects (DFE) for a given genotype represents the fitness changes brought about by all accessible mutations from that genotype. This should not be confused with the other common use of the term DFE, which refers to the fitness effects from past fixed mutations within a population. The DFE fundamentally governs the stochastic dynamics of evolution, making it a central focus in evolutionary biology.

Some studies have empirically measured the DFE in various organisms [5, 6, 7, 8, 9, 10] and proteins [11, 12], revealing that the DFE is typically unimodal, exhibiting a large deleterious tail and a smaller beneficial tail. Compared to the beneficial tail, a large deleterious tail is expected for a relatively well-adapted organism engaged in an adaptive walk toward a local fitness peak. At a local peak, by definition, all mutations are deleterious, resulting in a purely deleterious DFE.

The beneficial part of the distribution of fitness effects (BDFE) is particularly noteworthy because, in sufficiently large populations, deleterious mutations cannot fixate. Consequently, the BDFE often serves as the primary driver of evolution, with its shape determining the rate of adaptation. A seminal work by Orr [13] established that, under simple assumptions, the BDFE should follow an exponential distribution. This finding has been supported by numerous empirical studies across various organisms [5, 6, 11, 9], and further theoretical work [14]. Others, however, have reported measurements of non-exponential BDFEs [15]. The BDFE is often characterized by its mean, which is a measure of the average fitness effect of beneficial mutations. Orr makes two simple assumptions: first, that the fitness of all genotypes are drawn independently from some distribution that belongs to the Gumbel family of extreme value distributions, and second, that the organism is well-adapted to its environment, and as a result, not many beneficial mutations are available. Orr's first assumption is simple and may be approximately true in some cases, yet it is highly non-trivial. We shall discuss in later sections why this assumption is not valid under the models we investigate, yet the BDFE remains exponential in these models for other reasons.

Other empirical studies have sought to measure properties of the DFE and their functional relationship with fitness. Such relationships are often termed global epistasis (GE), where properties of the DFE depend solely on the fitness of the genotype, independent of any microscopic details. Many empirical investigations have identified a linear decreasing relationship between the DFE's mean and the genotype's fitness from which it is sampled [7, 16]. This serves as a simple mechanism of diminishing returns epistasis [17], where the epistatic interactions between fixed mutations and the genotypic background lead to a diminishing effect on the BDFE.

The Long-Term Evolution Experiment (LTEE), initiated by Richard Lenski in 1988, provides a powerful empirical framework to explore evolutionary dynamics over extended timescales. This ongoing experiment tracks 12 initially identical populations of *E. coli*, allowing them to evolve in identical environments under controlled

laboratory conditions. By periodically sampling and freezing cultures, the LTEE captures snapshots of evolutionary change, enabling retrospective analyses of genetic and phenotypic evolution. Over tens of thousands of generations, the LTEE has yielded profound insights into adaptation, mutation dynamics, epistasis, and historical contingency, offering an unparalleled opportunity to observe evolutionary processes in real-time and in remarkable detail [18].

Two recent studies, Couce et al. [9] and Ascensao et al. [19], conducted a detailed empirical analysis of DFEs in LTEE populations over time. Using deletion libraries, the authors of both studies sampled the DFE across generations for strains in the LTEE with exceptional coverage, revealing important insights into the evolution of the DFE. Couce et al. measured deletion libraries for the two ancestral strains (REL606 and REL 607) and for isolated clones from 10 out of the 12 evolved strains of the LTEE, at generations 2K, 15K, and 50K. Ascensao et al. measured deletion libraries for the ancestor (REL606, denoted as R) and two isolated clones from the ARA-2 population (denoted S and L) at generation 6.5K, for a number of different conditions. While some findings regarding the DFE aligned with previous observations, such as the overall shapes of the DFE and BDFE, others were unexpected. Notably, Couce et al. discovered that deletions that were beneficial (fitness effect > 0) in the ancestor (ARA+2) showed no bias toward being beneficial in evolved strains. In fact, the fitness effects of these deletions, measured in the evolved genotypic background, were indistinguishable from the overall DFE (2-sample KS test), suggesting that these mutations "forgot" their ancestral benefit and behaved like random samples from the evolved DFE. This phenomenon, which we term "scrambling", was also observed in reverse — for deletions that were beneficial in evolved strains, the fitness effects measured in the ancestral genotypic background were indistinguishable from the overall ancestral DFE. Although Ascensao et al. did not specifically address this phenomenon in their work, we also observed it in their data. Four different conditions from Ascensao et al. met the criteria for assessing scrambling, specifically those in which DFEs for all three strains (R, S, and L) were measured within the same experiment. For each of these conditions, we can measure the scrambling between the ancestor (R) and either of the evolved strains (S and L), resulting in a total of eight different measurements of possible scrambling. All eight measurements show similar scrambling behavior. In figure 1, we present data from both studies (Couce et al. and Ascensao et al.), where we arbitrarily chose one experiment (from eight) in Ascensao et al. to present here, The rest are presented in section 8.4.

To theoretically investigate the DFE, researchers often utilize fitness landscape models [21]. Prominent examples include Fisher's Geometric Model (FGM) [22], the Sherrington-Kirkpatrick (SK) spin-glass model [23], and the NK model [24], among others. These models typically provide a microscopic mapping between genotypes and their fitness, as seen with the SK and NK models, or a more abstract mapping, as in the case of FGM. Fitness landscape models enable the exploration of the evolutionary process, including the dynamics of adaptation, the shape of the DFE, and the relationship between fitness and genotype, among other aspects. FGM has been employed to approximate the DFE near a local fitness peak [25], study epistasis [26], and derive the distribution of beneficial fitness effects (BDFE) [27, 28]. The NK model has been used to analyze properties of fitness landscapes, including ruggedness and characterizing adaptive walks and fitness peaks [24, 29, 30]. The SK model has been used to explain fitness trajectories in the long-term evolution experiment [31], study epistasis [31, 32, 33],

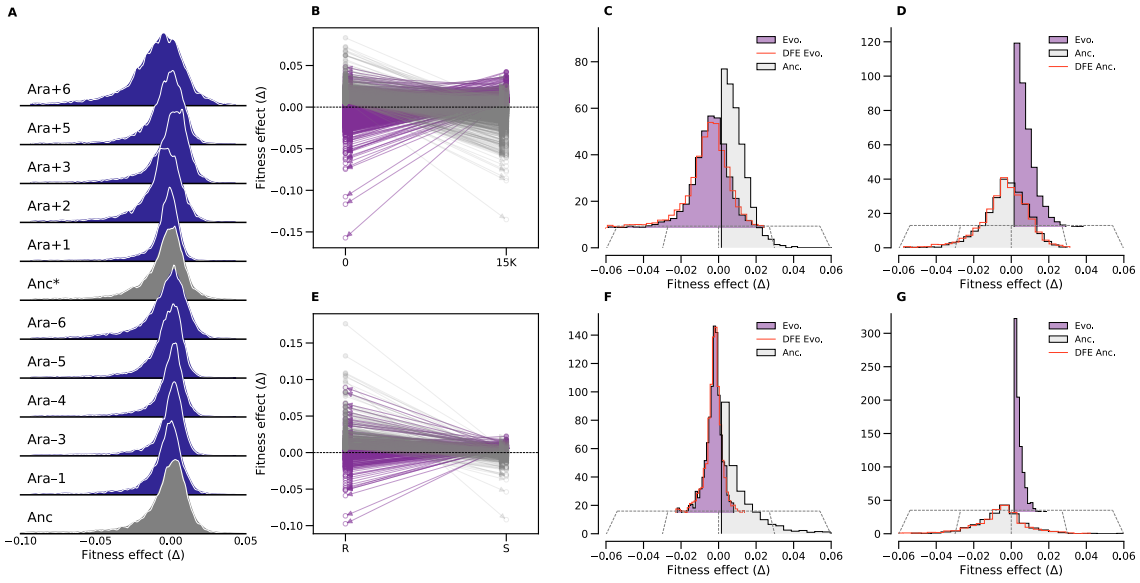

Figure 1: Couce et al. [9] data is presented in subfigures (A)—(D) (first row), and Ascensao et al. [19] data (for R and S clones from PQT experiment, as seen in the author's GitHub [20]) is presented in subfigures (E)—(G) (second row). All histograms are normalized to have unit area. (**A**) DFEs for 10 out of the 12 strains, as measured in Couce et al. Ancestors are in grey, evolved strains (generation 50K) are in blue. (**B**) Fitness effects of deletions that were beneficial at generation 0 (grey) and generation 15K (purple), respectively, measured at both genotypic backgrounds. Arrows connect pairs of points representing the same deletion in the two genotypic backgrounds, and indicate the direction of time. (**C**) Fitness effects of deletions that were beneficial for the ancestor (generation 0, grey), measured at the evolved genotypic background (generation 15K, purple). Also shown is the overall DFE of the evolved genotypic background (generation 15K, red). (**D**) Fitness effects of deletions that were beneficial for the evolved strain (generation 15K, purple), measured at the ancestral genotypic background (generation 0, grey). Also shown is the overall DFE of the ancestor (generation 0, red). (**E**) Fitness effects of deletions that were beneficial for R (generation 0, grey) and S (generation 6.5K, purple), respectively, measured at both genotypic backgrounds. Arrows connect pairs of points representing the same deletion in the two genotypic backgrounds, and indicate the direction of time. (**F**) Fitness effects of deletions that were beneficial for R (generation 0, grey), measured at the genotypic background of S (generation 6.5K, purple). Also shown is the overall DFE of S (generation 6.5K, red). (**G**) Fitness effects of deletions that were beneficial for S (generation 6.5K, purple), measured at the genotypic background of R (generation 0, grey). Also shown is the overall DFE of R (generation 0, red).

and study GE [34]. In this work, we will show that all qualitative properties of the DFE previously introduced, including the overall shape and dynamics of the DFE and BDFE, GE and scrambling, emerge naturally from the fitness landscape models we study. We also give analytical explanations for many of these properties, including scrambling.

2 Fitness Landscape Models

We aim to study the various properties of the DFE that are widely observed, discussed in the introduction 1. These include the dynamics of the DFE and BDFE: the unimodality of the DFE along with its distinct left skewness, the exponential shape of the BDFE, global epistasis, and the effect of "scrambling". To this end, we employ three of the most commonly utilized fitness landscape models, which we describe below.

2.1 Fisher's Geometric Model

Fisher's geometric model (FGM) is a highly studied fitness landscape model that captures many of the essential features of evolutionary dynamics, such as epistasis and pleiotropy (a phenomenon in which a single mutation affects a number of phenotypic traits) [26, 35]. One of the main attractions of FGM is its simplicity, where the model does not assume any specific genotype-to-fitness mapping, but rather focuses on the geometric nature of climbing a local fitness peak in a multidimensional space. In FGM, a phenotype is defined as a point $\boldsymbol{z} \in \mathbb{R}^n$ in phenotypic space, where each of the n dimensions corresponds to an independent phenotype under selection. FGM models adaptive walks towards a local fitness peak in this phenotypic space, rather than in genotypic space, and assumes that lower-dimensional continuous phenotypes can well-represent high-dimensional discrete genotypes. The fitness landscape over phenotypic space in FGM is Gaussian, with a single fitness peak at the origin. We consider the simplest version of FGM, where we assume the Gaussian fitness landscape is approximately isotropic, such that the fitness of any phenotype $\boldsymbol{z}$ is a function of only the distance from the origin

$$F(\boldsymbol{z}) := \exp\left(-\|\boldsymbol{z}\|^2\right), \tag{1}$$

where the model is built such that the optimal fitness is 1 and the lowest is 0. Mutations are modeled as additive random steps in phenotypic space

$$\boldsymbol{\delta} \sim \mathcal{N}\big(\mathbf{0}, \sigma^2 \mathbf{I}_n\big), \tag{2}$$

so that a phenotype $\boldsymbol{z}$ which undergoes a mutation $\boldsymbol{\delta}$ results in the phenotype $\boldsymbol{z} + \boldsymbol{\delta}$. Consequently, the magnitudes of mutations $\|\boldsymbol{\delta}\|$ are distributed as chi-squared with n degrees of freedom, and the direction of mutations is uniformly distributed over the unit sphere in $\mathbb{R}^n$. Usually in FGM, the DFE is generated by drawing a fixed number m of new random mutations for each step and calculating the fitness change for each one. To study the dynamics of individual mutations during an adaptive walk, we sample m mutations at initialization and keep them constant throughout the adaptive walk. This is a simple way of implementing a mechanism to allow track-

ing of the dynamics of individual mutational effects. We denote this set of m mutation vectors as $\{\boldsymbol{\delta}_i\}_{i=1}^m$, and the fitness effect of each mutation is

$$\Delta_i \coloneqq \exp\left(-\|\boldsymbol{z}+\boldsymbol{\delta}_i\|^2\right) - \exp\left(-\|\boldsymbol{z}\|^2\right), \tag{3}$$

where Δ_i changes during the adaptive walk as a function of the current displacement $\boldsymbol{z}$. Simulations of adaptive walks in FGM are initialized with a random displacement $\boldsymbol{z_0} \sim \mathcal{N}\left(\mathbf{0}, \sigma_0^2 \mathbf{I}_n\right)$ from the origin and m sampled mutations $\{\boldsymbol{\delta}_i\}_{i=1}^m$. Some works suggest that FGM emerges naturally from more fundamental principles, and also reinforce the isotropic assumption [35]. Dynamics of the adaptive walk are described in section 2.4. It is important to note that although FGM seems like a simple, continuous model, it is in practice a discrete model that is similar to the models we shall discuss below. At initialization, m mutations are sampled — and for a given initial displacement $\boldsymbol{z_0}$, there are only 2^m accessible points on the fitness landscape. Adaptive walks do not fully reach the origin, but rather continue until they reach a local fitness maximum, at which no mutations are beneficial. There are many local maxima in FGM, and the number increases exponentially with the number of mutations m [36]. More details on the underlying complexity of FGM can be found in [36].

2.2 The SK Model

Originating from spin-glass physics, the Sherrington-Kirkpatrick (SK) model [37] is a cornerstone model that exhibits essential features of complex systems, such as aging, disorder, frustration, and highly rugged, multi-peaked landscapes [38, 39]. The SK model, being one of the most studied models in statistical physics, has been utilized to understand phenomena in glasses and disordered systems in general. Due to its rich structure, the SK model has been used in various fields, including evolutionary biology, where it serves as a model for complex fitness landscapes. Unlike FGM, the SK model defines a specific genome-to-fitness mapping. In the SK model, a genome of length N is represented as a vector $\boldsymbol{\sigma} = (\sigma_1, \ldots, \sigma_N)$, where each element σ_i can take values $+1$ or -1. A mutation corresponds to flipping a single σ_i to $-\sigma_i$. The following genome-to-fitness mapping defines the SK model

$$\mathcal{F}(\boldsymbol{\sigma}) = \sum_{i=1}^{N} h_i \sigma_i + \frac{1}{2} \sum_{i,j=1}^{N} \sigma_i J_{ij} \sigma_j, \tag{4}$$

where —

- $h_i \sim \mathcal{N}\left(0, \sigma_h^2\right)$ represent local fields acting on σ_i (not to be confused with the so-called "local field distribution"). This is a form of additive fitness contributions that are independent of the rest of the genome. Each σ_i contributes $\pm|h_i|$ to fitness, depending on its alignment with the sign of h_i. Selection drives σ_i to align with their respective h_i.
- $J_{ij} \sim \mathcal{N}\left(0, \sigma_J^2\right)$ are couplings representing pair-wise epistatic interactions. $\boldsymbol{J}$ is a symmetric $N \times N$ matrix with $J_{ii} = 0$. These terms represent fitness contributions of σ_i which depend on the underlying

genomic background. σ_i are pushed to align with the sign of every $J_{ij}\sigma_j$ term through selection, yet these terms have differing signs and magnitudes, leading to a complex optimization process for each σ_i.

- $\sigma_h^2 = 1 - \beta$ and $\sigma_J^2 = \beta/N$, where the parameter $0 \leq \beta \leq 1$ controls the relative strength of epistatic interactions (second term in equation (4)) compared to the additive effects (first term in equation (4)), thereby tuning the landscape's ruggedness. For $\beta = 0$, the landscape has a single peak (where all σ_i align with their respective h_i), and for $\beta = 1$, the landscape is highly rugged with many local maxima. The $\sigma_J^2 \propto N^{-1}$ scaling ensures the fitness is extensive, i.e. $\mathcal{F} \propto N$.

The fitness effect of flipping σ_i is given by

$$\Delta_i := -2\sigma_i \left(h_i + \sum_{j=1}^{N} J_{ij}\sigma_j \right). \tag{5}$$

When applying the SK model to evolution, interpreting σ_i requires careful consideration. A direct mapping of σ_i to specific genetic units such as nucleotides or genes is, most likely, an oversimplification. The model's primary strength lies in capturing the emergent properties of the fitness landscape and the resultant evolutionary dynamics. If an analogy must be drawn, the binary σ_i values are most aptly compared to on-off switches for gene activity. This interpretation aligns well with the experimental approach of using deletion libraries to characterize the DFE. Notably, the DFE data from Couce et al. [9], the main motivation for this work, were obtained using deletion library techniques. Simulations of adaptive walks in the SK model are initialized with a random genotype vector $\boldsymbol{\sigma}$, a Gaussian random vector $\boldsymbol{h}$, and a Gaussian random matrix $\boldsymbol{J}$. Dynamics of the adaptive walk are described in section 2.4.

2.3 The NK Model

The NK model, introduced by Kauffman and Levin [24], is a canonical model for studying rugged fitness landscapes in evolutionary biology. In the NK model, as in the SK model, a genome of length N is represented as a vector $\boldsymbol{\sigma} = (\sigma_1, \ldots, \sigma_N)$, where each element σ_i can take values $+1$ or -1. In the NK model, the fitness contribution of each locus i is a function (denoted f_i) of its state σ_i and the states of exactly K other loci it interacts with. Typically, these K loci are chosen in a cyclic manner as $\sigma_{i+1}, \ldots, \sigma_{i+K}$, where indices are taken modulo N. The total fitness is the sum of the fitness contributions from all loci

$$F(\boldsymbol{\sigma}) = \frac{1}{N} \sum_{i=1}^{N} f_i(\sigma_i, \sigma_{i+1}, \ldots, \sigma_{i+K}). \tag{6}$$

Some interpretations of the NK model allow for any form of f_i. However, as the model was first introduced, the canonical implementation is the random NK model. In this version, the fitness contributions $f_i(\sigma_i, \sigma_{i+1}, \ldots, \sigma_{i+K})$

are random variables drawn independently from a Gaussian distribution

$$f_i(\sigma_i, \sigma_{i+1}, \ldots, \sigma_{i+K}) \sim \mathcal{N}(0, \sigma_f^2) \tag{7}$$

for each unique set of $\sigma_i, \sigma_{i+1}, \ldots, \sigma_{i+K}$ and for unique loci i. Thus, the parameter K controls the epistatic complexity and ruggedness of the fitness landscape. For $K = 0$, the fitness contributions are independent of each other, and the model reduces to a simple additive model. For $K = N - 1$, flipping any σ_i affects all other loci such that all f_i are redrawn, leading to a completely uncorrelated fitness landscape with maximal ruggedness. Mutations are represented as flipping a single σ_i to $-\sigma_i$, which redraws $K+1$ of the affected f_i, and the change in fitness is given by

$$\Delta_i \coloneqq \frac{1}{N} \sum_{j=i-K}^{i} f_j(\ldots, -\sigma_i, \ldots) - f_j(\ldots, \sigma_i, \ldots). \tag{8}$$

Simulations of adaptive walks in the NK model are initialized with a random genotype vector $\boldsymbol{\sigma}$, and Gaussian random fitness contributions $f_i(\sigma_i, \sigma_{i+1}, \ldots, \sigma_{i+K})$ for each unique locus i, and unique tuple of $\sigma_i, \sigma_{i+1}, \ldots, \sigma_{i+K}$. Dynamics of the adaptive walk are described in section 2.4.

2.4 Dynamics

In each model, we simulate the process of evolution as an adaptive walk until we reach a local fitness maximum, where no beneficial mutations are available. We work in the strong-selection weak-mutation (SSWM) regime [40], where we assume that fixation times of mutations are much shorter than the time it takes for beneficial mutations to appear. We can effectively coarse-grain over these short fixation time scales in this regime and treat the population as having a single genome. This regime has simple dynamics to simulate, where we have a single genome that fixes mutations in discrete time steps. In this work, we focus solely on relative progress in the adaptive walk, disregarding true time. True time could be incorporated by accounting for fixation times as a function of the fitness effect of mutations [40], but this is not required for our purposes. We take the approximation of the population being large enough such that deleterious mutations do not fixate, and we only consider beneficial mutations. The probability p_Δ in our simulations to choose (fixate) a mutation with fitness effect Δ, at any time step, is given by —

$$p_\Delta \propto \begin{cases} \Delta & \Delta > 0 \\ 0 & \text{otherwise} \end{cases}, \tag{9}$$

where fixation probability being approximately linear in the fitness effect is a known result in evolutionary theory [41].

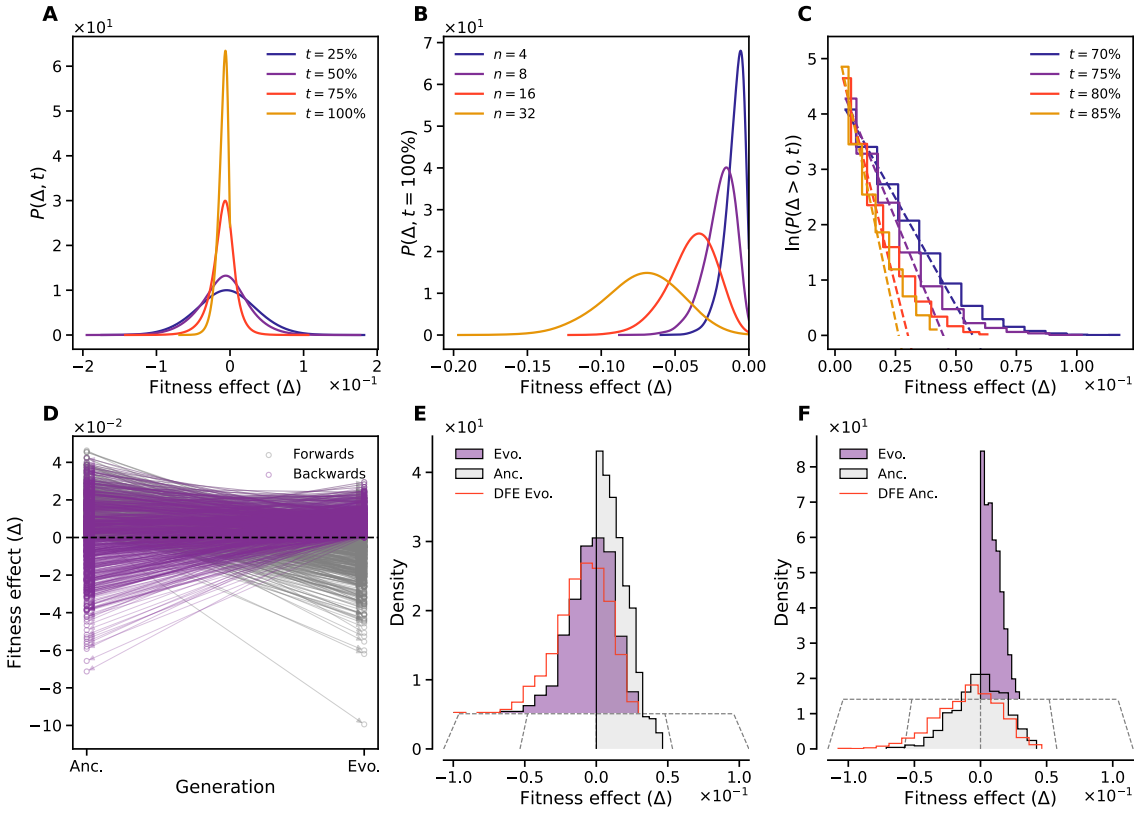

Figure 2: Simulation results for adaptive walks in the isotropic FGM; the adaptive walks were performed from a random initial position until a local fitness peak was reached. Parameter values are $m = 2000$, $\sigma = 0.05$, and, except for (B), $n = 4$. All values of the number of steps t are normalized to a percentage of the total number of steps (mutations) during the adaptive walk, where specifically Anc. (ancestor) refers to $t = 70\%$ and Evo. (evolved) refers to $t = 80\%$ of completed steps. Subfigures (A)—(C) (first row) were created by averaging over 100 independent simulations, and show aspects of overall DFE dynamics. Subfigures (D)—(F) (second row) show different aspects of scrambling for a single, typical simulation of an adaptive walk. (**A**) The DFE during different stages of the adaptive walk. (**B**) The DFE at a local 1-flip maxima for different values of n. (**C**) The BDFE during different stages of the adaptive walk; note the semi-logarithmic scale. (**D**) Fitness effects of mutations that were beneficial for the ancestor (grey) and evolved (purple) generations, respectively, measured at both genotypic backgrounds. Arrows connect pairs of points representing the same mutation in the two genotypic backgrounds, and indicate the direction of time. (**E**) Fitness effects of mutations that were beneficial for the ancestor generation (grey), measured at the evolved generations' genotypic background (purple). Also shown is the overall DFE of the evolved genotypic background (red). (**F**) Fitness effects of mutations that were beneficial for the evolved generation (purple), measured at the ancestral generations' genotypic background (grey). Also shown is the overall DFE of the ancestor genotypic background (red).

3 FGM Results

In FGM, the DFE at the fitness peak in the isotropic case can be approximated to first order in $\|\boldsymbol{\delta}\|^2$ as

$$F(\boldsymbol{\delta}) - F(\mathbf{0}) = \exp\left(-\|\boldsymbol{\delta}\|^2\right) - 1 \approx -\sum_{i=1}^{n} \delta_i^2, \tag{10}$$

where $\delta_i \sim \mathcal{N}(0, \sigma^2)$ are Gaussian distributed, so equation (10) results in a chi-squared distribution. We emphasize that both the magnitude of mutations ($\|\boldsymbol{\delta}\|^2$) and the approximation of the DFE at the fitness peak (equation (10)) are chi-squared distributed. Previous works have approximated the DFE near the fitness peak [25], and derived it fully in the general non-isotropic case [35]. In section 8.1.1, we present a simplified derivation of the DFE in the isotropic case, characterizing it as a variation on a non-central chi-squared distribution with a non-centrality parameter dependent solely on the distance from the origin. These results are exact only in the infinite m limit, and approximate for finite m due to finite sampling. During a typical adaptive walk in FGM, the DFE starts as approximately Gaussian with zero mean when far from the fitness peak, and gradually transitions to a left-skewed distribution, as illustrated in figure 2A. At the fitness peak, the DFE follows a chi-squared distribution as described by equation (10), for which

$$P(|\Delta| \ll 1) \propto \Delta^{\frac{n}{2}-1}. \tag{11}$$

As can be understood from equation (11), as n increases, the slope of the DFE at the origin decreases, and for $n > 2$ at the fitness peak, $P(\Delta) \to 0$ as $|\Delta| \to 0$. Additionally, at the fitness peak, the gap between the DFE's maximum and the origin widens with increasing n, as shown in figure 2B, which plots DFEs at the fitness peak for increasing values of n. This results from the growing overall magnitude of mutations with increasing n, so each mutation at the peak becomes a larger step away from the origin. This growing neutral mutation gap phenomenon is also reproduced in the SK and NK models, and we discuss its biological implications in section **??**. In figure 2C, we can see the BDFE plotted at different times during the adaptive walk, where it seems to converge to an exponential distribution as the adaptive walk approaches the fitness peak. Previous theoretical work by Orr has shown that the BDFE in FGM should be exponentially distributed [27], though Orr shows this under slightly different conditions (Orr assumes a fixed mutation size $\|\boldsymbol{\delta}\|^2 = r$). We show that under our particular simulation conditions, this result still holds. In figures 2D — 2F, we see a demonstration of scrambling in FGM, which is consistently reproduced in simulations of adaptive walks. In the framework of FGM, we can understand scrambling analytically. At any point $\boldsymbol{z}$ in an adaptive walk, a mutation is beneficial if it satisfies the condition

$$\|\boldsymbol{z} + \boldsymbol{\delta}\| < \|\boldsymbol{z}\|. \tag{12}$$

Therefore, the geometric picture for beneficial mutations is that at any point $\boldsymbol{z}$ in the adaptive walk, the set of all beneficial mutations is the set of vectors that point to all points in the open ball of radius $\|\boldsymbol{z}\|$ centered at $-\boldsymbol{z}$.

Alternatively, the set of beneficial mutations can be described in a ray formulation as

$$\|\boldsymbol{\delta}\| < -2\|\boldsymbol{z}\|cos\theta, \tag{13}$$

where θ is the angle between the displacement vector $\boldsymbol{z}$ and the mutation vector $\boldsymbol{\delta}$. This picture defines the maximal magnitude of a mutation that is still beneficial as a function of θ, and gives the same result as the geometric picture. For instance, mutations pointing directly towards the origin have $\theta = \pi$, and in order to be beneficial must have a magnitude of less than $2\|\boldsymbol{z}\|$. Mutations orthogonal to the displacement vector, which have $\theta = \frac{\pi}{2}$, cannot be beneficial. Thus, the set of all beneficial mutations forms an n-dimensional hypersphere that shrinks linearly as the distance from the origin decreases. At the large $\boldsymbol{z}$ limit relative to the mean mutation size ($\|\boldsymbol{z}\| \gg n\sigma^2$), all mutations in the angular range of $\frac{\pi}{2} < \theta \leq \pi$ are beneficial, regardless of their magnitude.

Now, denote the subset of mutations that are beneficial at some arbitrary displacement $\boldsymbol{z_0}$ as $\mathcal{B}_{\boldsymbol{z_0}}$. The fitness effects of mutations in this set change as the adaptive walk progresses and the displacement $\boldsymbol{z}$ is no longer at the initial value of $\boldsymbol{z_0}$, yet the set itself remains unchanged. At the isotropic fitness peak, all mutations are deleterious and their direction is irrelevant to their fitness effect — their fitness effect depends only on their magnitude, which is chi-squared distributed (equation (2)). The fitness effects themselves, at the peak, are also distributed approximately chi-squared (equation (10)). Let us consider first the limiting case of large $\boldsymbol{z_0}$ relative to the mean mutation magnitude, $\|\boldsymbol{z_0}\|^2 \gg n\sigma^2$. Because the question of whether mutations belong to $\mathcal{B}_{\boldsymbol{z_0}}$ or not depends only on their direction in this limit, the distribution of the magnitudes of mutations in $\mathcal{B}_{\boldsymbol{z_0}}$ is chi-squared distributed. This leads, in the large $\boldsymbol{z_0}$ limit, to the DFE of $\mathcal{B}_{\boldsymbol{z_0}}$ at the fitness peak being indistinguishable from the total DFE at the fitness peak. The convergence of the DFE of $\mathcal{B}_{\boldsymbol{z_0}}$ along the adaptive walk — from being completely beneficial at $\boldsymbol{z_0}$ (and unlike the total DFE at $\|\boldsymbol{z_0}\| \gg n\sigma^2$ which is approximately Gaussian with mean 0), to being indistinguishable from the total DFE at the fitness peak — happens smoothly as the adaptive walk progresses. However, for $\mathcal{B}_{\boldsymbol{z_0}}$ of $\|\boldsymbol{z_0}\|$ not in the large limit, there exists a magnitude cutoff for beneficial mutations, where no mutation with a magnitude larger than $2\|\boldsymbol{z_0}\|$ has a possibility of being beneficial (inequality (13)). In this regime, the distribution of magnitudes of mutations in $\mathcal{B}_{\boldsymbol{z_0}}$ is no longer chi-squared distributed, and is more similar, roughly speaking, to a truncated chi-squared distribution. This results in the DFE of $\mathcal{B}_{\boldsymbol{z_0}}$ at the fitness peak being increasingly different from the total DFE at the fitness peak, as $\|\boldsymbol{z_0}\|$ decreases. So, in essence, scrambling depends on how advanced along the adaptive walk the organism is when the BDFE is initially measured. An important note to be made in regard to the arguments above is that they are not only valid for the subset of beneficial mutations — one can also consider the set of deleterious mutations at $\boldsymbol{z_0}$, and the same arguments apply. Coincidentally, Couce et al. observed scrambling not only for beneficial mutations, but also for deleterious mutations. We also observe scrambling for deleterious mutations in our simulations.

The convergence process described above can primarily be explained by changes in the radial component of the displacement vector alone, without the necessity of considering its angular components. Throughout the preceding analysis, all outcomes depended exclusively on the magnitude $\|\boldsymbol{z}\|$, independent of its direction $\hat{\boldsymbol{z}}$. We term this component of scrambling as *biased scrambling*, which captures how the autocorrelation of fitness effects

of mutations changes during the biased motion (adaptive walk) towards the fitness peak. However, the results depicted in figures 2E and 2F clearly illustrate effects that biased scrambling alone cannot explain. Specifically, the scenario depicted in figure 2F, where previously deleterious mutations become beneficial, cannot happen through radial motion alone. This statement can be understood by considering again inequality (13), where if we assume radial motion alone, θ remains constant and $\|\boldsymbol{z}\|$ decreases every step in the adaptive walk — leading only to the possibility of the transition of mutations from beneficial to deleterious (due to their magnitude being too large), but not the other way around. The above understanding implies a distinct, additional mechanism involving angular components. In FGM, adaptive walks progress systematically toward the fitness peak, with each adaptive step constrained to either maintain or reduce the radial distance $\|\boldsymbol{z}\|$. The components of the mutation vectors $\boldsymbol{\delta}$ are drawn independently, and while mutations are selected for based on their radial component, the $n-1$ angular components of the mutations are ignored by the selection process. Consequently, the selection process results in the dynamics of the $n-1$ angular components of the displacement vector $\boldsymbol{z}$ undergoing a random walk on an $n-1$ spherical surface of changing radius $\|\boldsymbol{z}\|$, where the directions of mutations are uniformly distributed on the surface of the sphere. This process, which we term *unbiased scrambling* and expand on analytically in section 8.1.2, is largely independent of the process of biased scrambling and only coupled to it through the radius of the sphere that the angular components of the displacement vector $\boldsymbol{z}$ are constrained to. Thus, biased and unbiased scrambling are two complementary mechanisms through which the fitness effects of mutations become decorrelated in adaptive evolution. Biased scrambling reflects the convergence of evolutionary paths toward fitness peaks, while angular scrambling captures the stochastic, unbiased exploration of the landscape's angular dimensions.

4 SK Results

The results of our SK simulations are illustrated in figure 3. It can be seen that qualitatively, the model seems to recreate all results discussed in sections **??** and 3. In figure 3A, we see the same qualitative behavior of the DFE as in FGM, where the DFE is approximately Gaussian with zero mean initially when far from the fitness peak, and gradually transitions to a left-skewed distribution as the adaptive walk progresses. In figure 3B, we see the DFE at a local fitness peak for different values of β. The DFE in the SK model corresponds to the local field distribution in spin-glass physics, a concept that has been extensively studied [42, 43, 44, 45, 46]. A notable characteristic of the local field distribution in spin glasses is the local field gap, which has been a focus of significant interest in prior studies. A distinction is made between "true gaps" and "pseudo gaps" in the literature, where true gaps are characterized by some critical value $\Delta_c \neq 0$ such that $P(\Delta) = 0$ for all $|\Delta| < |\Delta_c|$, implying the system is highly stable to small perturbations — flipping many of the spins does not change the energy of the system. Pseudo gaps, on the other hand, are characterized by $P(\Delta) \to 0$ as $\Delta \to 0$, meaning that there is a suppression of small local fields but not a complete absence of them. Some of the spins in the system feel weak effective fields, but their density vanishes near zero. This kind of behavior of local extremum being on the cusp of instability is known as marginal stability [47], and is an important feature of the SK model where the local field gap is linear,

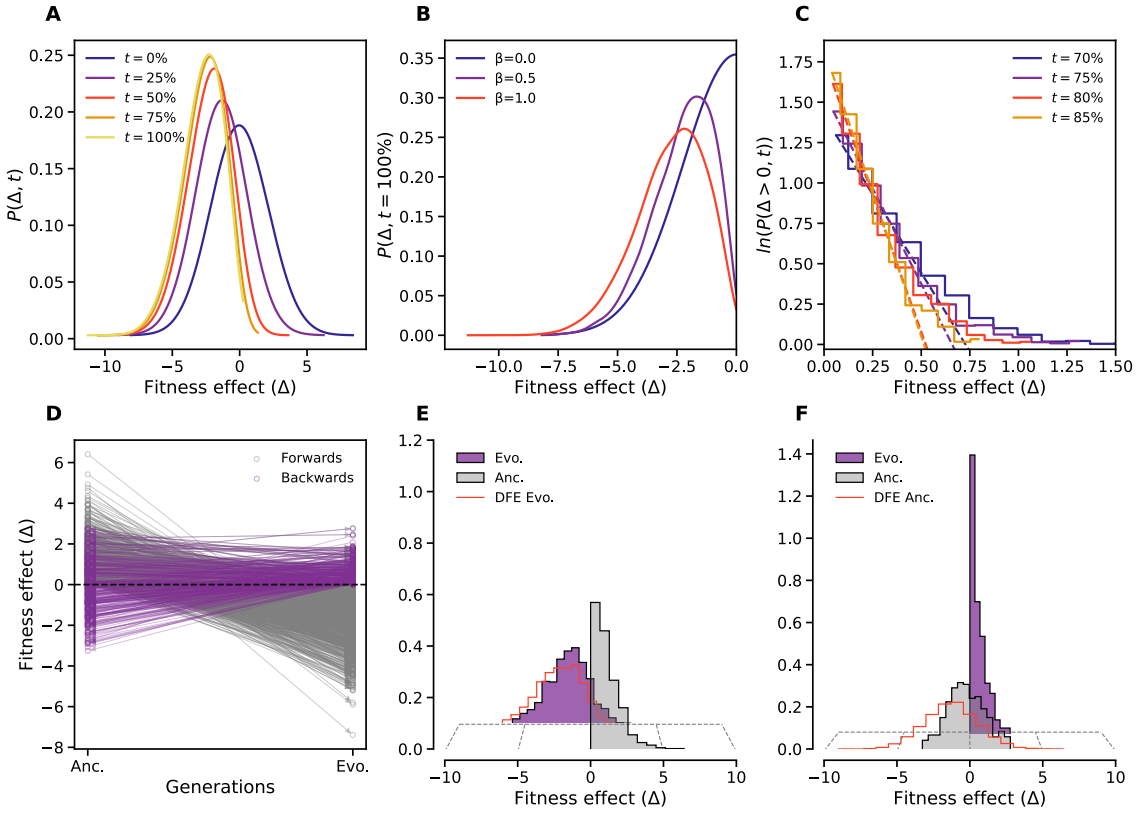

Figure 3: Simulation results for adaptive walks in the SK model; the adaptive walk was performed from a random initial genome until a local fitness peak was reached. Plots are for values $N = 4000$ and, except for (B), $\beta = 1$. All values of the number of steps t are normalized to a percentage of the total number of steps (mutations) during the adaptive walk, where specifically Anc. (ancestor) refers to $t = 25\%$ and Evo. (evolved) refers to $t = 50\%$ of completed steps. Subfigures (A)—(C) (first row) were created by averaging over 50 independent simulations, and show aspects of overall DFE dynamics. Subfigures (D)—(F) (second row) show different aspects of scrambling for a single, typical simulation of an adaptive walk. (**A**) The DFE during different stages of the adaptive walk. (**B**) The DFE at a local fitness peak for different values of β. (**C**) The BDFE during different stages of the adaptive walk; note the semi-logarithmic scale. (**D**) Fitness effects of mutations that were beneficial for the ancestor (grey) and evolved (purple) generations, respectively, measured at both genotypic backgrounds. Arrows connect pairs of points representing the same mutation in the two genotypic backgrounds, and indicate the direction of time. (**E**) Fitness effects of mutations that were beneficial for the ancestor generation (grey), measured at the evolved generations' genotypic background (purple). Also shown is the overall DFE of the evolved genotypic background (red). (**F**) Fitness effects of mutations that were beneficial for the evolved generation (purple), measured at the ancestral generations' genotypic background (grey). Also shown is the overall DFE of the ancestor genotypic background (red).

i.e., $P(\Delta) \propto \Delta$ for small Δ. Arguments for the linear scaling have been introduced in previous works on the subject [47]. In figure 3C, it seems qualitatively that the BDFE converges to an exponential distribution as the adaptive walk progresses. In section 8.2, we show that under a late time approximation, the BDFE converges to an Airy distribution, rather than an exponential distribution — although they are qualitatively similar and hard to distinguish in practice. We expand on this in section 8.2. In figures 3D—3F, we demonstrate scrambling in the SK model. Although we demonstrate scrambling only for the BDFE, simulations show scrambling also for the deleterious part of the DFE, as in FGM. Unlike in FGM, we have not found an exact analytical explanation for scrambling in the SK model.

5 NK results

The results of our NK simulations are illustrated in figure 4. It can be seen that qualitatively, all results discussed in the previous sections are reproduced in the NK model as well. In figure 4A, we see that the DFE is initially approximately Gaussian with zero mean when far from the fitness peak, and gradually transitions to a left-skewed distribution as the adaptive walk progresses. In figure 4B, we see the DFE at a local 1-flip maximum for different values of K. As in FGM and the SK model, we observe an increase in the neutral mutation pseudo-gap with increasing K. Numerical results indicate that the small Δ behavior of the DFE at a local 1-flip maximum exhibits a non-trivial dependence on K. Specifically, we find that $P(\Delta \ll 1) \propto \Delta^{f(K)}$, with $f(K)$ being a non-linear function of K. In figure 4C, we see that the BDFE seems to converge to an exponential distribution as the adaptive walk progresses; this convergence becomes stronger with increasing K. In figures 4D—4F, we demonstrate scrambling in the NK model. Although we demonstrate scrambling only for the BDFE, scrambling is recreated by simulations for the deleterious part of the DFE as well, as seen in the other models and as observed by Couce et al. and Asencao et al. Unlike FGM, we have not found analytical explanations for these behaviors in the NK model.

6 Global Epistasis

While not addressed in Couce et al., global epistasis (GE) is a well-established phenomenon closely tied to the DFE [48]. The term GE has been used with varying definitions across different studies; in this work, we define it as the direct functional relationship between specific properties of the DFE and fitness. For example, experimental observations have shown that the mean of the DFE exhibits a decaying linear relationship with fitness [7, 16], which is the most commonly discussed form of GE, though other forms may also be considered. In section 8.3, we present full analytical derivations for the mean of the DFE across all three fitness landscape models. All three models exhibit a decaying linear relationship between the mean of the DFE and fitness, and we summarize these results in this section, where we denote F as the current fitness, and all model parameters are defined in section 2. For FGM, we find

$$\langle \Delta \rangle \approx -n\sigma^2 F, \tag{14}$$

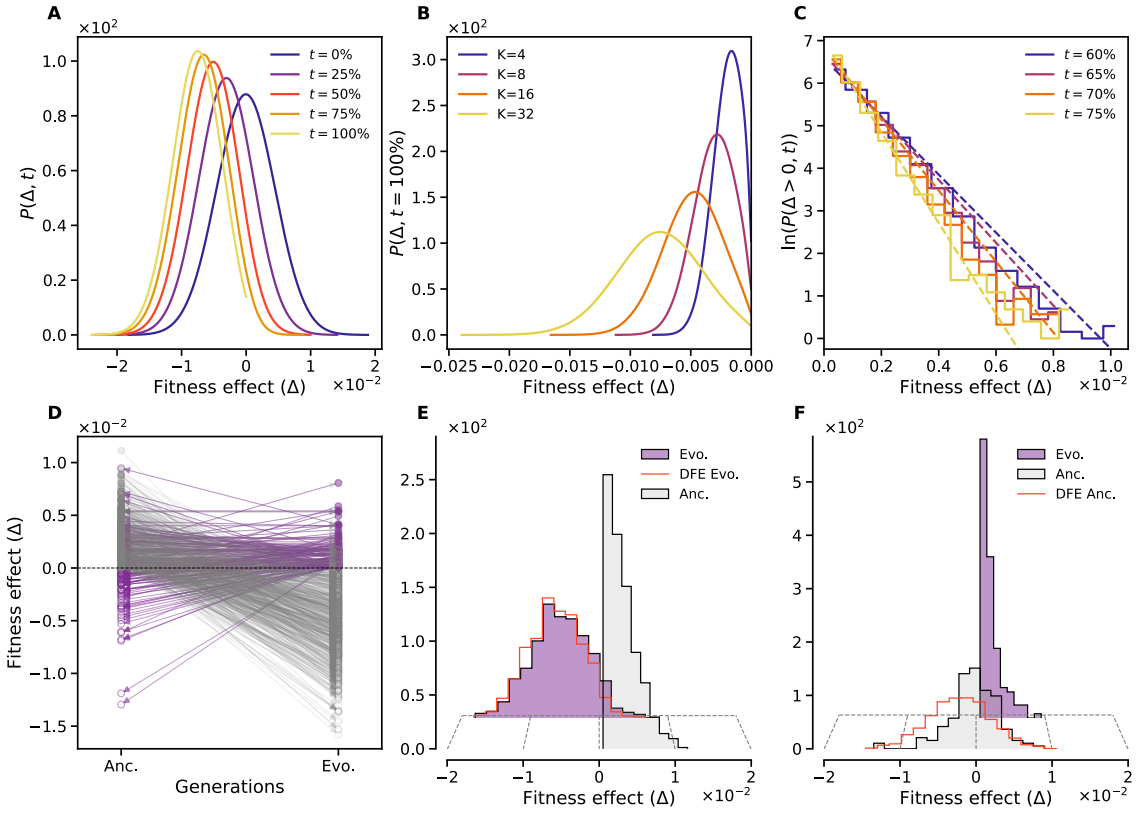

Figure 4: Simulation results for adaptive walks in the NK model; the adaptive walk was performed from a random initial genome until a local fitness peak was reached Plots are for values $N = 2000$, $\sigma_f = 1$, and except for (B), $K = 32$. All values of the number of steps t are normalized to a percentage of the total number of steps (mutations) during the adaptive walk, where specifically Anc. (ancestor) refers to $t = 25\%$ and Evo. (evolved) refers to $t = 50\%$ of completed steps. Subfigures (A)—(C) (first row) were created by averaging over 50 independent simulations, and show aspects of overall DFE dynamics. Subfigures (D)—(F) (second row) show different aspects of scrambling for a single, typical simulation of an adaptive walk. (**A**) The DFE during different stages of the adaptive walk. (**B**) The DFE at a local fitness peak for different values of K. (**C**) The BDFE during different stages of the adaptive walk; note the semi-logarithmic scale. (**D**) Fitness effects of mutations that were beneficial for the ancestor (grey) and evolved (purple) generations, respectively, measured at both genotypic backgrounds. Arrows connect pairs of points representing the same mutation in the two genotypic backgrounds, and indicate the direction of time. (**E**) Fitness effects of mutations that were beneficial for the ancestor generation (grey), measured at the evolved generations' genotypic background (purple). Also shown is the overall DFE of the evolved genotypic background (red). (**F**) Fitness effects of mutations that were beneficial for the evolved generation (purple), measured at the ancestral generations' genotypic background (grey). Also shown is the overall DFE of the ancestor genotypic background (red).

where $n\sigma^2$ is exactly the mean magnitude of mutations $\boldsymbol{\delta}$ in FGM. In the SK model, for $\beta = 0$ we find

$$\langle \Delta \rangle = -\frac{2}{N} F, \tag{15}$$

and for $\beta = 1$ we find

$$\langle \Delta \rangle = -\frac{4}{N} F, \tag{16}$$

where in section 8.3 we derive this for a more general form of β. In the NK model, we find

$$\langle \Delta \rangle = -\frac{K+1}{N} F. \tag{17}$$

. Interestingly, all models exhibit a linear relationship between the mean of the DFE and fitness, with a negative slope.

7 Conclusion

In all three models, which constitute three of the most widely used fitness landscape models, we qualitatively recreate all experimental results discussed in section 1. The characteristic shape of the DFE described by Couce et al. and others — a unimodal distribution with a long deleterious tail and a short beneficial tail — is reproduced across all three models. The dynamics of the DFE across all three models are similar, with initial DFEs being approximately Gaussian with zero mean far from the fitness peak, and becoming increasingly left-skewed (negative) as the adaptive walk progresses. The initial distance from the fitness peak sets the initial shape of the DFE, with closer proximity to the peak resulting in a more left-skewed initial DFE that deviates from a Gaussian distribution. Experimental results, including those by Couce et al., consistently show that the DFE is initially somewhat left-skewed, reflecting the organisms' high level of adaptation to their environment and their proximity to a fitness peak. Based on the models presented in this work, it is reasonable to infer that in experimental settings where organisms are poorly adapted to their environment, The initial DFE would exhibit a more Gaussian-like distribution (in other words, DFEs are, at worst, symmetrical around zero — but never more positive or right-skewed leaning than that). An important aspect of the DFE dynamics is the pseudo-gap of neutral mutations at a fitness peak, as detailed in previous sections, with the gap size increasing with the relevant parameters in each model. This result has biological implications — neutral mutations are almost absent at the fitness peak, preventing the genome from undergoing neutral adaptation at this stage. Increasing relevant parameters in each model further reduces the prevalence of near-neutral deleterious mutations at the fitness peak. The probability of a deleterious mutation fixing is negligible in sufficiently large populations. Consequently, once a fitness peak is reached, the genome remains static for extended periods, without even neutral adaptation, until either a deleterious mutation is fixed, such as in stochastic tunneling [33], or external factors alter the landscape. This finding could help illuminate the "paradox of stasis" [49], which is the apparent contradiction between the observation that some species show little or no evolutionary change over long periods of time, despite the expectation that nat-

ural selection and genetic drift should continually drive adaptation and change. We understand this pseudo-gap analytically in FGM as the increasing number of degrees of freedom of the chi-squared distribution at the peak (see section 3). However, it should be noted that for $n \leq 2$ in FGM, neutral mutations are generally available at the fitness peak. Although this scenario is most likely unrealistic in nature, where organisms undergo selection in several phenotypic categories, both in survival and reproduction, evolutionary experiments may isolate specific phenotypic properties to such an extent that the category of landscapes with $n \leq 2$ may be relevant.

Expanding on the observed dynamics of the DFE, we turn to the exponential BDFE observed by Couce et al. and others, which, despite being considered a canonical result in evolutionary theory due to Orr [13], relies on assumptions invalid for correlated landscapes, as previously stated in section 1. Yet, in all three models, the BDFE seems to converge approximately to an exponential form as the adaptive walk approaches a local fitness peak. The SK model shows slightly different analytical behavior with some reasonable approximations, discussed in section 8.2. This behavior is not easily observed on a half-log scale and appears exponential, as illustrated in figure 3. Simulations of the BDFE in the SK model show greater agreement with Airy (KS test p-value of 0.6) than with exponential (KS test p-value of 0.2), though statistical agreement with both distributions is acceptable.

The phenomenon we termed "scrambling" is consistently reproduced across all three models. This process is understood best analytically in the context of FGM. Scrambling results in an inability to predict future fitness effects of mutations based on their prior effects. Nonetheless, this does not preclude parallelism, where identical mutations fix across different lineages, as observed in Couce et al., from occurring in clonal evolution experiments. Given that the initial DFEs are identical across clones, the possibility of the same mutations fixing in different clones remains feasible and depends on the fitness effects. However, scrambling may influence evolutionary dynamics such that a clone's mutational trajectory, after diverging slightly from the majority trajectory, could increasingly deviate in the short term. Within the framework of fitness landscape models, this divergence does not prevent clones from converging to the same fitness peak but indicates that distinct mutational trajectories may lead each clone to the shared peak.

From a broader perspective, all three models, despite their differences, exhibit remarkably similar qualitative behavior. This raises the question of whether an analytical equivalence exists among them, or more specifically, if an equivalence exists between DFEs in all three models. If such an equivalence exists, the analytical insights derived from FGM could potentially be extended to interpret the results of the SK and NK models. The framework of FGM is based on a minimal set of assumptions: an isotropic Gaussian fitness peak and mutations represented as constant additive vectors on the fitness landscape, with entries drawn independently from a Gaussian distribution. Yet, the deceptively simple FGM hides a more complex underlying structure of a Hopfield network [36], which is a special case of a spin-glass system. FGM may be reformulated in the following way:

$$\boldsymbol{z} = \boldsymbol{z_0} + \sum_{i=1}^{m} \boldsymbol{\delta_i} \tau_i, \tag{18}$$

where $\boldsymbol{z_0}$ is the initial displacement and $\tau_i \in \{0, 1\}$ are dynamic indicator variables, all set initially to zero.

Flipping τ_i to 1 corresponds to moving by mutation i in the landscape, where the τ_i are free to flip back from 1 to 0 as well, if advantageous. The magnitude of the displacement is then

$$\|\boldsymbol{z}\|^2 = \|\boldsymbol{z_0}\|^2 + 2\boldsymbol{z_0}\sum_{i=1}^{m}\boldsymbol{\delta_i}\tau_i + \sum_{i=1}^{m}(\boldsymbol{\delta_i}\cdot\boldsymbol{\delta_j})\,\tau_i\tau_j. \tag{19}$$

We can approximate the fitness $F = \exp(-\|\boldsymbol{z}\|^2)$ in FGM near the peak to first order in $\|\boldsymbol{z}\|^2$ as

$$\exp(-\|\boldsymbol{z}\|^2) \approx -\sum_{i=1}^{m} l_i\tau_i - \sum_{i=1}^{m} M_{ij}\tau_i\tau_j \tag{20}$$

Where we define $M_{ij} =: (\boldsymbol{\delta_i}\cdot\boldsymbol{\delta_j})$ and $l_i =: 2\boldsymbol{z_0}\cdot\boldsymbol{\delta_i}$, and neglect the constant term $-\|\boldsymbol{z_0}\|^2 - 1$. The form in equation (20) seems identical to the SK model, yet there is a key difference — the statistics of the coupling matrices are different in the two models. The coupling matrix J_{ij} in the SK model is defined by $N(N-1)/2$ independent Gaussian variables (GOE matrix) and has Wigner eigenvalue statistics, while the coupling matrix in FGM, M_{ij}, is defined by $m \times n$ independent Gaussian variables (Wishart matrix) and has Marchenko–Pastur eigenvalue statistics. So, it is clear that FGM and SK are not equivalent, yet similar. It is also clear that the NK model is not equivalent to either FGM or SK, as it is not fully connected. The question remains how all three models can exhibit such similar qualitative behavior of the DFE (including overall dynamics, exponential BDFE, GE, and scrambling) along adaptive walks, despite their differences. Although we do not provide an answer to this question in this work, we speculate that some, if not all, of the qualitative behaviors observed are general features of spin-like systems.

8 Appendix

8.1 FGM Analysis

8.1.1 DFE Derivation

In FGM as defined in section 2.1, the fitness effect of a mutation $\boldsymbol{\delta}$ for a walker at point $\boldsymbol{z}$ is given by

$$F(\boldsymbol{z}+\boldsymbol{\delta}) - F(\boldsymbol{z}) = e^{-\|\boldsymbol{z}+\boldsymbol{\delta}\|^2} - e^{-\|\boldsymbol{z}\|^2}. \tag{21}$$

Due to the isotropic condition, we assume that $\boldsymbol{z} = r\boldsymbol{e_1}$. Thus, we have that

$$\|\boldsymbol{z}+\boldsymbol{\delta}\|^2 = (r+\delta_1)^2 + \sum_{i=2}^{n}\delta_i^2 \tag{22}$$

is distributed as a non-central chi-squared distribution with n degrees of freedom and non-centrality parameter $\lambda = r^2/\sigma^2$. The non-central chi-squared distribution is defined as

$$f(u,r) = \frac{1}{2\sigma^2}\exp\Big(-\frac{u+r^2}{2\sigma^2}\Big)\Big(\frac{u}{r^2}\Big)^{\frac{n}{4}-\frac{1}{2}} \times I_{\frac{n}{2}-1}\Big(\frac{r\sqrt{u}}{\sigma^2}\Big), \tag{23}$$

where I_ν is the modified Bessel function of the first kind. The fitness is given by transforming the non-central chi-squared distribution to form of the fitness effect, as in equation (21) which results in

$$P(\Delta,r) = \frac{1}{2\sigma^2(\Delta+e^{-r^2})} \times \exp\left(-\frac{r^2-\ln(\Delta+e^{-r^2})}{2\sigma^2}\right)\left(\frac{-\ln(\Delta+e^{-r^2})}{r^2}\right)^{\frac{n}{4}-\frac{1}{2}} \times I_{\frac{n}{2}-1}\left(\frac{r}{\sigma^2}\sqrt{-\ln(\Delta+e^{-r^2})}\right), \tag{24}$$

which is defined on $-e^{-r^2} \leq \Delta \leq 1-e^{-r^2}$.

8.1.2 Unbiased Scrambling

Here, we give a partial argument for backwards scrambling. Consider an adaptive walker undergoing isotropic Brownian motion in $\mathbb{R}^n$ with diffusion coefficient D. Let $X_t \in \mathbb{R}^n$ denote the position of the walker, and decompose it into radial and angular components as

$$X_t = R(t)U_t, \quad \text{where } R(t) = \|X_t\|, \quad U_t = \frac{X_t}{\|X_t\|} \in S^{n-1}.$$

Based on the fixation process, we use a simplifying assumption on the radial evolution of the walker where we assume the radius evolves linearly over a time interval $[0,\Delta t]$ as

$$R(t) = R_1 + \frac{R_2-R_1}{\Delta t}t \quad t \in [0,\Delta t], \tag{25}$$

with $R_1 > R_2$ as the initial and final radii of the segment of the adaptive walk we are interested in. The angular component U_t evolves on the unit sphere S^{n-1} and satisfies the Itô SDE

$$dU_t = -\frac{(n-1)D}{R(t)^2}\,U_t\,dt + \frac{\sqrt{2D}}{R(t)}\,(I - U_tU_t^\top)\,dW_t, \tag{26}$$

where W_t is standard Brownian motion in $\mathbb{R}^n$. The drift term arises from the Itô correction associated with the projection onto the sphere. We are interested in computing the autocorrelation of the angular unit vector over

the interval $[0, \Delta t]$

$$C(\Delta t) \coloneqq \mathbb{E}[U_{\Delta t} \cdot U_0].$$

To compute this, we consider the conditional expectation $m(t) = \mathbb{E}[U_t \mid U_0]$, which satisfies the deterministic differential equation obtained by averaging the SDE

$$\frac{d}{dt} m(t) = -\frac{(n-1)D}{R(t)^2}\, m(t), \tag{27}$$

where $m(0) = U_0$. Solving equation (27) yields:

$$m(t) = U_0 \exp\left(-(n-1)D \int_0^t \frac{ds}{R(s)^2}\right). \tag{28}$$

Substituting equation (25) gives:

$$\int_0^{\Delta t} \frac{ds}{R(s)^2} = \frac{\Delta t}{R_1 R_2}$$

The angular autocorrelation is

$$\begin{aligned} C(\Delta t) &= \mathbb{E}[\mathbb{E}[U_{\Delta t}|U_0] \cdot U_0] \\ &= \mathbb{E}\left[U_0 \cdot U_0 \exp\left(-\frac{(n-1)D}{R_1 R_2}\Delta t\right)\right], \end{aligned}$$

and $U_0 \cdot U_0 = 1$, therefore:

$$C(\Delta t) = \exp\left(-\frac{(n-1)D}{R_1 R_2}\Delta t\right) \tag{29}$$

Thus, vectors diffusing on the sphere become orthogonal to their initial position exponentially fast, and the rate increases with dimensionality.

8.2 SK Analysis

Previous works have studied Fokker-Planck equations for the SK model extensively [45, 46]. Adopting the approach of Eastham et al. [46], we use the following Fokker-Planck equation for the SK model

$$\begin{aligned} \frac{\partial P(\Delta, t)}{\partial t} =& \frac{|\Delta|}{q(t)} \left(P(-\Delta, t)\Theta(-\Delta) - P(\Delta, t)\Theta(\Delta)\right) \\ & - c\frac{\partial P(\Delta, t)}{\partial \Delta} + \frac{D}{2}\frac{\partial^2 P(\Delta, t)}{\partial \Delta^2} \end{aligned}, \tag{30}$$

where

- $q(t) \coloneqq \int_0^\infty \Delta P(\Delta, t) d\Delta$ is for probability normalization purposes,

- $\Theta(\Delta)$ is the Heaviside step function.

Notice we added a $|\Delta|$ factor to the flipping term, which is a consequence of the SSWM fixation probabilities. Now, define the term "drifts" as

$$d_{ij} \coloneqq 4\sigma_i J_{ij} \sigma_j. \tag{31}$$

Flipping a random σ_j will affect Δ_i as

$$\Delta_i \to \Delta_i + d_{ij}, \tag{32}$$

where we neglect the correlations that build up in the spins, and treat equation (32) as steps in a random walk. This is a biased random walk, as the mean of these steps ($\langle d_{ij} \rangle$ for j such that $\Delta_j > 0$) is non-vanishing, which can be seen as follows

$$\begin{aligned} \mathbb{E}[d_{ij} | \Delta_j > 0] &= \frac{1}{N r(t)} \sum_{i, j | \Delta_j > 0} 4\sigma_i J_{ij} \sigma_j \\ &= -2\frac{\mathbb{E}[P(\Delta > 0, t)]}{N} - \sum_{j | \Delta_j > 0} \frac{4 h_j \sigma_j}{r(t) N}, \end{aligned} \tag{33}$$

where $r(t)$ is the number of beneficial mutations at time t. Note that the magnitude of both terms in 33 decay to zero with time. We denote

$$c(t) \coloneqq -2\mathbb{E}[P(\Delta > 0, t)] - \sum 4 h_j \sigma_j / r(t), \tag{34}$$

and approximate it for simplicity as a constant, such that the total mean of drifts is c/N. Observe that as β decreases from 1 to 0, c decays from $-2\mathbb{E}[P(\Delta > 0, t)]$ to 0. Numerical solutions of (30) seem to recreate the DFE dynamics observed in the SK model quite accurately. For these numerical solutions, we find the drift term much smaller than the diffusion and flip terms, even for constant c. Thus, we can confidently write the effective equation for the late times and $\Delta > 0$, based on equation (30), assuming an almost stationary phase, as

$$-\Delta P(\Delta, t) + q(t) \frac{D}{2} \frac{\partial^2 P(\Delta, t)}{\partial \Delta^2} = 0, \tag{35}$$

of which the solution for $\Delta > 0$ is the Airy function of the first kind

$$P(\Delta) \propto \mathrm{Ai}\left(\frac{\Delta}{(q(t) D/2)^{1/3}} \right). \tag{36}$$

If we swap the linear fixation probabilities for a positive uniform distribution, equation (35) becomes (with the appropriate change to $q(t)$)

$$P(\Delta) = q(t) \frac{D}{2} \frac{\partial^2 P(\Delta, t)}{\partial \Delta^2}, \tag{37}$$

which has the solution for $\Delta > 0$

$$P(\Delta) \propto \exp\left(\frac{-\Delta}{\sqrt{q(t)\frac{D}{2}}}\right). \tag{38}$$

KS tests show greater agreement with the Airy function ($p = 0.6$) than the exponential ($p = 0.2$).

8.3 Global Epistasis

8.3.1 FGM

The mean of the DFE in FGM (equation (24)) can be calculated as

$$\langle \Delta \rangle = (1 + 2\sigma^2)^{-\frac{n}{2}} \exp\Big(-\frac{r^2}{1 + 2\sigma^2}\Big) \; - \; e^{-r^2}, \tag{39}$$

and assuming $\sigma \ll 1$ we can approximate equation (39) as

$$\langle \Delta \rangle \approx -n\sigma^2 F(r) \tag{40}$$

where $F(r) = e^{-r^2}$ is the fitness during the adaptive walk. Interestingly, the decay rate of the mean relative to the fitness is exactly the mean magnitude of mutations $\langle \|\boldsymbol{\delta}\|^2 \rangle = n\sigma^2$.

8.3.2 SK Model

For the SK model, the linear decaying relationship between the mean of the DFE and the fitness is a known theoretical result [34]. Here, we add a slightly more detailed derivation with the exact scaling, for a general p-spin SK model, which we define below. The SK model we define in section 2 as a special case of a spin-glass system, combining 1-point interactions and 2-point interactions, the former being the interactions of the spins σ_i with the local fields vector h_i, and the latter being the interactions of the spins with each other through the coupling matrix J_{ij}. In general, we can define a p-dimensional tensor $J_{i_1 \cdots i_p}$ that describes the interactions of p spins, and this is known as the p-spin SK model. The fitness of the p-spin SK model can be written as

$$F(\sigma) = \frac{1}{p!} \sum_{i_1=1}^{N} \sum_{i_2=1}^{N} \cdots \sum_{i_p=1}^{N} J_{i_1 \cdots i_p} \, \sigma_{i_1} \cdots \sigma_{i_p}, \tag{41}$$

where $J_{i_1 \cdots i_p}$ is fully symmetric under index permutations, and has zero diagonal such that if any $i_n = i_m$ then $J_{i_1 \cdots i_p} = 0$. For spin k, we have the local field

$$l_k^{(p)} \coloneqq \frac{1}{(p-1)!} \sum_{i_1=1}^{N} \cdots \sum_{i_{p-1}=1}^{N} J_{k\, i_1 \cdots i_{p-1}} \, \sigma_{i_1} \cdots \sigma_{i_{p-1}}, \tag{42}$$

such that flipping spin k results in a fitness change

$$\Delta_k := -2\sigma_k \, l_k^{(p)}. \tag{43}$$

The mean of the DFE is given by

$$\langle \Delta \rangle = \frac{1}{N} \sum_{k=1}^{N} \Delta_k, \tag{44}$$

and we can see that using equation (42) we have

$$\begin{aligned} \sum_{k=1}^{N} \sigma_k \, l_k^{(p)} &= \frac{1}{(p-1)!} \times \\ \sum_{k=1}^{N} \sum_{i_1,\ldots,i_{p-1}} & J_{k\, i_1 \cdots i_{p-1}} \, \sigma_k \, \sigma_{i_1} \cdots \sigma_{i_{p-1}}. \end{aligned} \tag{45}$$

Now, change the indices such that $k \to i_1$ and $i_n \to i_{n+1}$ for the remaining indices, and we have

$$\langle \Delta \rangle = -\frac{2p}{N} F, \tag{46}$$

where F is the fitness during the adaptive walk.

8.3.3 NK Model

In equation (8), there are two different types of f_i contributing to fitness change — the f_i sampled for the current genome $\boldsymbol{\sigma}$, and the newly sampled f_i for the new genome with $\sigma_i \to -\sigma_i$. The newly sampled f_i are Gaussian with mean zero, as defined in equation (7). The current f_i are a result of an adaptive walk and thus are biased, and have approximately the form of some extreme value distribution. Taking the mean, we have

$$\langle \Delta \rangle = \frac{1}{N} \sum_{k=1}^{N} \Delta_k = -\frac{1}{N} \sum_{i=1}^{N} \frac{1}{N} \sum_{j=i-K}^{i} f_j(\boldsymbol{\sigma}),$$

where we used the fact that the newly sampled f_i average to zero. Finally, we get

$$\langle \Delta \rangle = -\frac{K+1}{N} F, \tag{47}$$

where F is the fitness during the adaptive walk.

8.4 Ascensao et al. Data

In this section, we present data from Ascensao et al. [19]. Presented are data from four different experiments from a total of nine experiments done by Ascensao et al. Each experiment involved a different growth condition, where we chose to present data from all experiments where the DFEs of the R, S, and L strains were measured. Other experiments measured data for S and L strains, but not R, and this data does not allow for the analysis of scrambling.

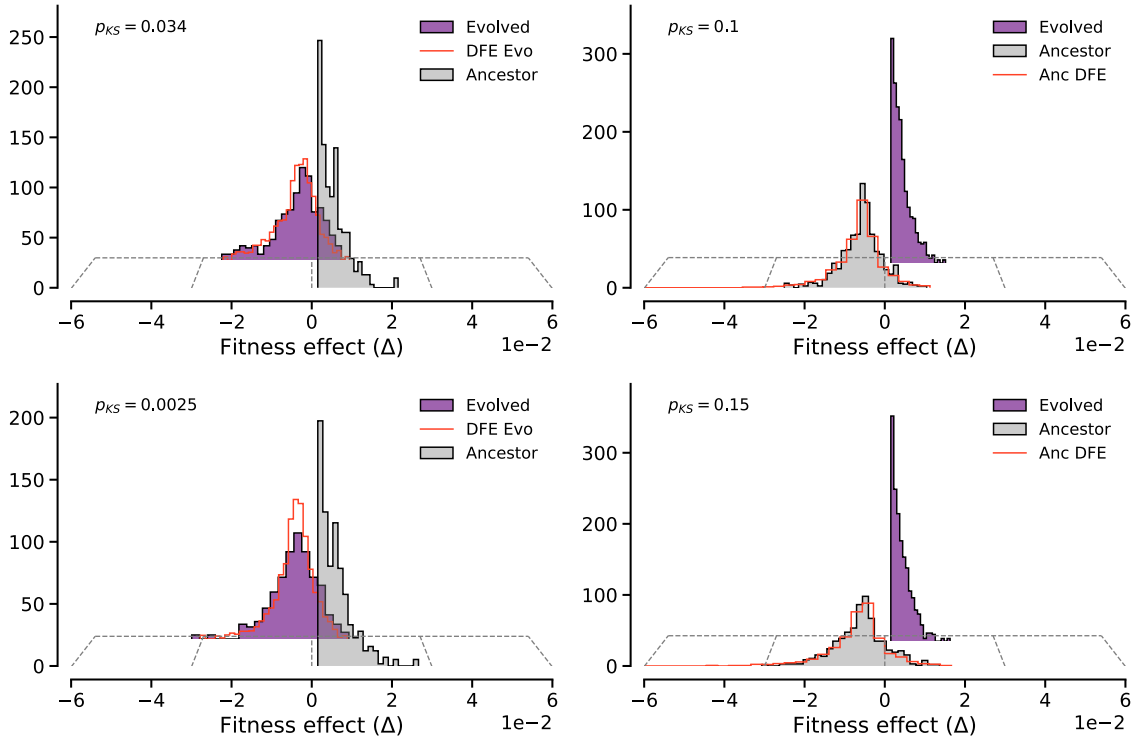

Figure 5: Data from Ascensao et al. [19]. DFEs measured for monocultures of R, S, and L strains. The p-values of 2-sample KS tests between the propagated DFE and the total DFE are shown in the top left corner of each panel. (**A**) Fitness effects of deletions that were beneficial for R (generation 0, grey), measured at the genotypic background of L (generation 6.5K, purple). Also shown is the overall DFE of L (generation 6.5K, red). (**B**) Fitness effects of deletions that were beneficial for L (generation 6.5K, purple), measured at the genotypic background of R (generation 0, grey). Also shown is the overall DFE R (generation 0, red). (**C**) Fitness effects of deletions that were beneficial for R (generation 0, grey), measured at the genotypic background of S (generation 6.5K, purple). Also shown is the overall DFE of S (generation 6.5K, red). (**D**) Fitness effects of deletions that were beneficial for S (generation 6.5K, purple), measured at the genotypic background of R (generation 0, grey). Also shown is the overall DFE R (generation 0, red).

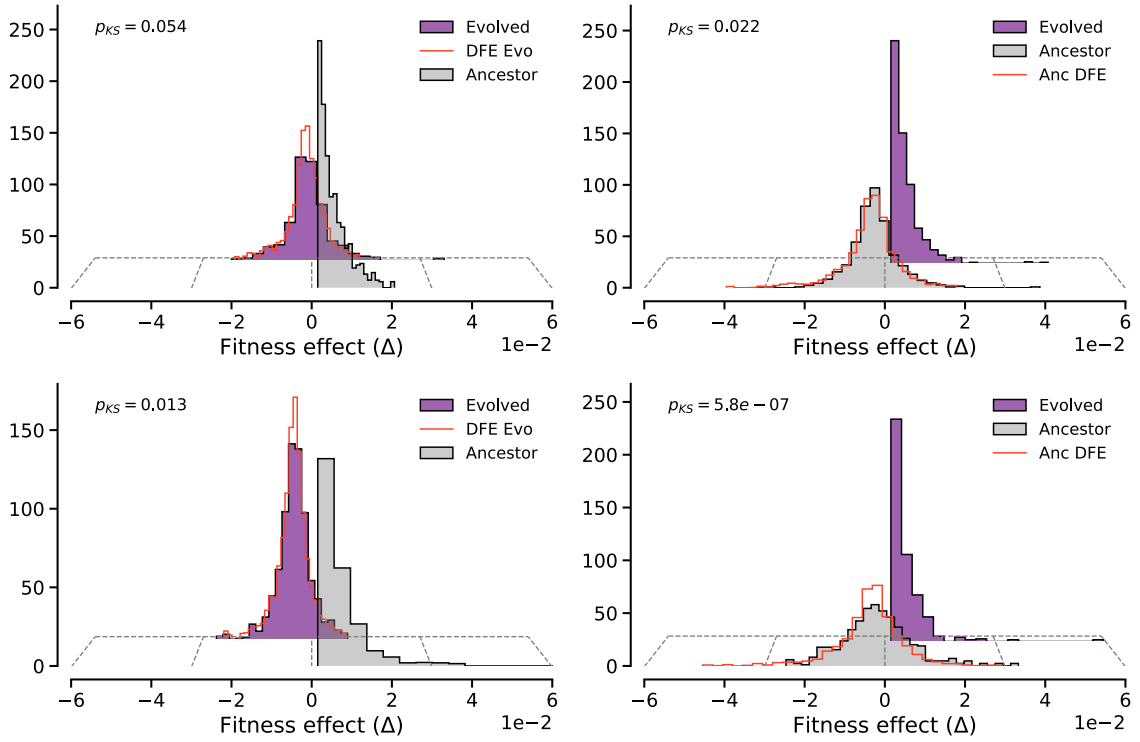

Figure 6: Data from Ascensao et al. [19]. DFEs measured for monocultures of R, S, and L strains - exponential growth in actate. The p-values of 2-sample KS tests between the propagated DFE and the total DFE are shown in the top left corner of each panel. (**A**) Fitness effects of deletions that were beneficial for R (generation 0, grey), measured at the genotypic background of L (generation 6.5K, purple). Also shown is the overall DFE of L (generation 6.5K, red). (**B**) Fitness effects of deletions that were beneficial for L (generation 6.5K, purple), measured at the genotypic background of R (generation 0, grey). Also shown is the overall DFE R (generation 0, red). (**C**) Fitness effects of deletions that were beneficial for R (generation 0, grey), measured at the genotypic background of S (generation 6.5K, purple). Also shown is the overall DFE of S (generation 6.5K, red). (**D**) Fitness effects of deletions that were beneficial for S (generation 6.5K, purple), measured at the genotypic background of R (generation 0, grey). Also shown is the overall DFE R (generation 0, red).

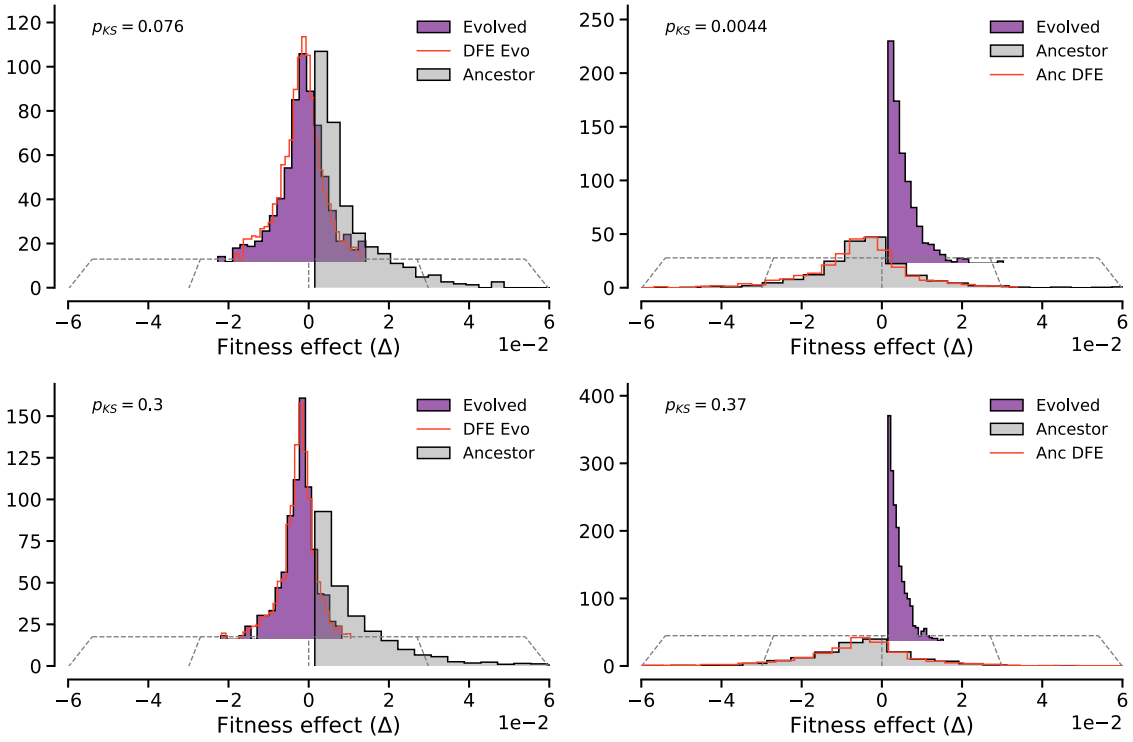

Figure 7: Data from Ascensao et al. [19]. DFEs measured for monocultures of R, S, and L strains - exponential DM25 growth. The p-values of 2-sample KS tests between the propagated DFE and the total DFE are shown in the top left corner of each panel. (**A**) Fitness effects of deletions that were beneficial for R (generation 0, grey), measured at the genotypic background of L (generation 6.5K, purple). Also shown is the overall DFE of L (generation 6.5K, red). (**B**) Fitness effects of deletions that were beneficial for L (generation 6.5K, purple), measured at the genotypic background of R (generation 0, grey). Also shown is the overall DFE R (generation 0, red). (**C**) Fitness effects of deletions that were beneficial for R (generation 0, grey), measured at the genotypic background of S (generation 6.5K, purple). Also shown is the overall DFE of S (generation 6.5K, red). (**D**) Fitness effects of deletions that were beneficial for S (generation 6.5K, purple), measured at the genotypic background of R (generation 0, grey). Also shown is the overall DFE R (generation 0, red).

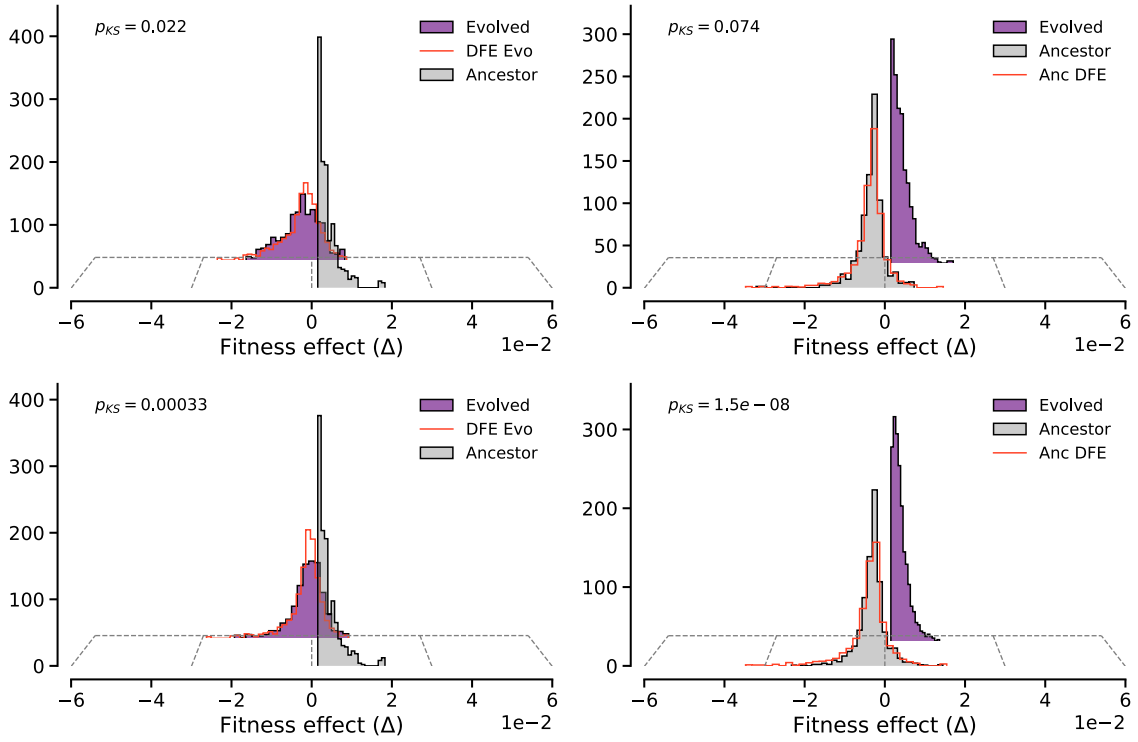

Figure 8: Data from Ascensao et al. [19]. DFEs measured for monocultures of R, S, and L strains - 1/10x dilution rate. The p-values of 2-sample KS tests between the propagated DFE and the total DFE are shown in the top left corner of each panel. (**A**) Fitness effects of deletions that were beneficial for R (generation 0, grey), measured at the genotypic background of L (generation 6.5K, purple). Also shown is the overall DFE of L (generation 6.5K, red). (**B**) Fitness effects of deletions that were beneficial for L (generation 6.5K, purple), measured at the genotypic background of R (generation 0, grey). Also shown is the overall DFE R (generation 0, red). (**C**) Fitness effects of deletions that were beneficial for R (generation 0, grey), measured at the genotypic background of S (generation 6.5K, purple). Also shown is the overall DFE of S (generation 6.5K, red). (**D**) Fitness effects of deletions that were beneficial for S (generation 6.5K, purple), measured at the genotypic background of R (generation 0, grey). Also shown is the overall DFE R (generation 0, red).

References

[1] P. Alberch. "From genes to phenotype: dynamical systems and evolvability." *Genetica*, volume 84(1):p. 5–11 (1991). ISSN 1573-6857.

[2] S. M. Wadgymar, S. Sheth, E. Josephs, M. DeMarche, J. Anderson. "Defining fitness in evolutionary ecology." *International Journal of Plant Sciences*, volume 185(3):p. 218–227 (2024). ISSN 1537-5315.

[3] N. Hanna, B. Parfait, D. Vidaud, M. Vidaud. "Mécanismes et conséquences des mutations." *médecine/sciences*, volume 21(11):p. 969–980 (2005). ISSN 1958-5381.

[4] G. P. Wagner, J. Zhang. "The pleiotropic structure of the genotype–phenotype map: the evolvability of complex organisms." *Nature Reviews Genetics*, volume 12(3):p. 204–213 (2011). ISSN 1471-0064.

[5] R. Kassen, T. Bataillon. "Distribution of fitness effects among beneficial mutations before selection in experimental populations of bacteria." volume 38(4):pp. 484–488. ISSN 1061-4036. Place: United States.

[6] M. Imhof, C. Schlötterer. "Fitness effects of advantageous mutations in evolving *Escherichia coli* populations." *Proceedings of the National Academy of Sciences*, volume 98(3):pp. 1113–1117 (2001). ISSN 0027-8424, 1091-6490.

[7] M. S. Johnson, A. Martsul, S. Kryazhimskiy, M. M. Desai. "Higher-fitness yeast genotypes are less robust to deleterious mutations." *Science*, volume 366(6464):pp. 490–493 (2019).

[8] S. F. Elena, L. Ekunwe, N. Hajela, S. A. Oden, R. E. Lenski. "Distribution of fitness effects caused by random insertion mutations in Escherichia coli." R. C. Woodruff, J. N. Thompson, eds., "Mutation and Evolution," volume 7, pp. 349–358. Springer Netherlands, Dordrecht (1998). ISBN 978-94-010-6193-3 978-94-011-5210-5. Series Title: Contemporary Issues in Genetics and Evolution.

[9] A. Couce, A. Limdi, M. Magnan, S. V. Owen, C. M. Herren, R. E. Lenski, O. Tenaillon, M. Baym. "Changing fitness effects of mutations through long-term bacterial evolution." *Science*, volume 383(6681):p. eadd1417 (2024).

[10] G. Bell. "Experimental genomics of fitness in yeast." *Proceedings of the Royal Society B: Biological Sciences*, volume 277(1687):pp. 1459–1467 (2010). ISSN 0962-8452, 1471-2954.

[11] E. E. Wrenbeck, L. R. Azouz, T. A. Whitehead. "Single-mutation fitness landscapes for an enzyme on multiple substrates reveal specificity is globally encoded." *Nature Communications*, volume 8(1):p. 15695 (2017). ISSN 2041-1723.

[12] A. Acevedo, L. Brodsky, R. Andino. "Mutational and fitness landscapes of an RNA virus revealed through population sequencing." *Nature*, volume 505(7485):pp. 686–690 (2014). ISSN 1476-4687.

[13] H. A. Orr. "The distribution of fitness effects among beneficial mutations." volume 163(4):pp. 1519–1526. ISSN 0016-6731. Place: United States.

[14] A. Barlukova, I. M. Rouzine. "The evolutionary origin of the universal distribution of mutation fitness effect." *PLOS Computational Biology*, volume 17(3):p. e1008822 (2021). ISSN 1553-7358.

[15] D. R. Rokyta, C. J. Beisel, P. Joyce, M. T. Ferris, C. L. Burch, H. A. Wichman. "Beneficial fitness effects are not exponential for two viruses." *Journal of Molecular Evolution*, volume 67(4):p. 368–376 (2008). ISSN 1432-1432.

[16] S. M. Ardell, A. Martsul, M. S. Johnson, S. Kryazhimskiy. "Environment-independent distribution of mutational effects emerges from microscopic epistasis." *Science*, volume 386(6717):pp. 87–92 (2024).

[17] M. J. Wiser, N. Ribeck, R. E. Lenski. "Long-term dynamics of adaptation in asexual populations." *Science*, volume 342(6164):pp. 1364–1367 (2013).

[18] J. E. Barrick, R. E. Lenski. "Genome dynamics during experimental evolution." *Nature Reviews Genetics*, volume 14(12):p. 827–839 (2013). ISSN 1471-0064.

[19] J. A. Ascensao, K. M. Wetmore, B. H. Good, A. P. Arkin, O. Hallatschek. "Quantifying the local adaptive landscape of a nascent bacterial community." *Nature Communications*, volume 14(1) (2023). ISSN 2041-1723.

[20] J. Ascensão. "S-l-rel606-barseq: Analysis pipeline for rel606 barseq data." `https://github.com/joaoascensao/S-L-REL606-BarSeq` (2025).

[21] H. A. Orr. "The genetic theory of adaptation: a brief history." *Nature Reviews Genetics*, volume 6(2):pp. 119–127 (2005). ISSN 1471-0056, 1471-0064.

[22] R. A. Fisher. *The genetical theory of natural selection*. Clarendon Press (1930).

[23] D. Sherrington, S. Kirkpatrick. "Solvable Model of a Spin-Glass." *Physical Review Letters*, volume 35(26):pp. 1792–1796 (1975). ISSN 0031-9007.

[24] S. Kauffman, S. Levin. "Towards a general theory of adaptive walks on rugged landscapes." *Journal of Theoretical Biology*, volume 128(1):pp. 11–45 (1987). ISSN 00225193.

[25] G. Martin, T. Lenormand. "A general multivariate extension of fisher's geometrical model and the distribution of mutation fitness effects across species." *Evolution*, volume 60(5):pp. 893–907 (2006). ISSN 0014-3820, 1558-5646.

[26] G. Martin, S. F. Elena, T. Lenormand. "Distributions of epistasis in microbes fit predictions from a fitness landscape model." *Nature Genetics*, volume 39(4):pp. 555–560 (2007). ISSN 1061-4036, 1546-1718.

[27] H. A. Orr. "The distribution of fitness effects among beneficial mutations in fisher's geometric model of adaptation." *Journal of Theoretical Biology*, volume 238(2):pp. 279–285 (2006). ISSN 00225193.

[28] G. Martin, T. Lenormand. "The Distribution of Beneficial and Fixed Mutation Fitness Effects Close to an Optimum." *Genetics*, volume 179(2):pp. 907–916 (2008). ISSN 1943-2631.

[29] S. A. Kauffman, E. D. Weinberger. "The NK model of rugged fitness landscapes and its application to maturation of the immune response." *Journal of Theoretical Biology*, volume 141(2):pp. 211–245 (1989). ISSN 00225193.

[30] R. Durrett, V. Limic. "Rigorous results for the N K model." *The Annals of Probability*, volume 31(4) (2003). ISSN 0091-1798.

[31] N. M. Boffi, Y. Guo, C. H. Rycroft, A. Amir. "How microscopic epistasis and clonal interference shape the fitness trajectory in a spin glass model of microbial long-term evolution." *eLife*, volume 12:p. RP87895 (2024). ISSN 2050-084X.

[32] G. Pedruzzi, A. Barlukova, I. M. Rouzine. "Evolutionary footprint of epistasis." *PLOS Computational Biology*, volume 14(9):p. e1006426 (2018). ISSN 1553-7358.

[33] Y. Guo, M. Vucelja, A. Amir. "Stochastic tunneling across fitness valleys can give rise to a logarithmic long-term fitness trajectory." *Science Advances*, volume 5(7):p. eaav3842 (2019).

[34] G. Reddy, M. M. Desai. "Global epistasis emerges from a generic model of a complex trait." *eLife*, volume 10:p. e64740 (2021). ISSN 2050-084X.

[35] G. Martin. "Fisher's geometrical model emerges as a property of complex integrated phenotypic networks." *Genetics*, volume 197(1):pp. 237–255 (2014). ISSN 1943-2631.

[36] S. Hwang, S.-C. Park, J. Krug. "Genotypic complexity of fisher's geometric model." *Genetics*, volume 206(2):p. 1049–1079 (2017). ISSN 1943-2631.

[37] D. Sherrington, S. Kirkpatrick. "Solvable model of a spin-glass." *Phys. Rev. Lett.*, volume 35:pp. 1792–1796 (1975).

[38] V. M. D. Oliveira, J. F. Fontanari. "Landscape statistics of the p -spin Ising model." *Journal of Physics A: Mathematical and General*, volume 30(24):pp. 8445–8457 (1997). ISSN 0305-4470, 1361-6447.

[39] G. Parisi. "On the statistical properties of the large time zero temperature dynamics of the sk model." *Fractals*, volume 11(supp01):pp. 161–171 (2003).

[40] M. A. Nowak. *Evolutionary Dynamics: Exploring the Equations of Life*. Harvard University Press (2006). ISBN 9780674023383.

[41] M. Kimura. "On the probability of fixation of mutant genes in a population." *Genetics*, volume 47(6):pp. 713–719 (1962). ISSN 1943-2631.

[42] R. G. Palmer, C. M. Pond. "Internal field distributions in model spin glasses." *Journal of Physics F: Metal Physics*, volume 9(7):pp. 1451–1459 (1979). ISSN 0305-4608.

[43] M. Thomsen, M. F. Thorpe, T. C. Choy, D. Sherrington, H. J. Sommers. "Local magnetic field distributions. III. Disordered systems." *Physical Review B*, volume 33(3):pp. 1931–1947 (1986). ISSN 0163-1829.

[44] S. Boettcher, H. G. Katzgraber, D. Sherrington. "Local field distributions in spin glasses." *Journal of Physics A: Mathematical and Theoretical*, volume 41(32):p. 324007 (2008). ISSN 1751-8113, 1751-8121.

[45] H. Horner. "Time Dependent Local Field Distribution and Metastable States in the SK-Spin-Glass." *The European Physical Journal B*, volume 60(4):pp. 413–422 (2007). ISSN 1434-6028, 1434-6036. ArXiv:0707.2714 [cond-mat].

[46] P. R. Eastham, R. A. Blythe, A. J. Bray, M. A. Moore. "Mechanism for the failure of the Edwards hypothesis in the Sherrington-Kirkpatrick spin glass." *Physical Review B*, volume 74(2):p. 020406 (2006). ISSN 1098-0121, 1550-235X.

[47] M. Müller, M. Wyart. "Marginal stability in structural, spin, and electron glasses." *Annual Review of Condensed Matter Physics*, volume 6(Volume 6, 2015):pp. 177–200 (2015). ISSN 1947-5462.

[48] J. Diaz-Colunga, A. Skwara, K. Gowda, R. Diaz-Uriarte, M. Tikhonov, D. Bajic, A. Sanchez. "Global epistasis on fitness landscapes." *Philosophical Transactions of the Royal Society B: Biological Sciences*, volume 378(1877):p. 20220053 (2023). ISSN 0962-8436, 1471-2970.

[49] J. T. Stroud, W. C. Ratcliff. "Long-term studies provide unique insights into evolution." *Nature*, volume 639(8055):pp. 589–601 (2025). ISSN 0028-0836, 1476-4687.